Received: 30 July 2021 | Revised: 19 October 2021 | Accepted: 18 November 2021

DOI: 10.1111/pce.14240

ORIGINAL ARTICLE

Plant, Cell & Environment | WILEY

A conserved clathrin-coated vesicle component, OsSCYL2, regulates plant innate immunity in rice

Yao Yao[1,2] | Jihua Zhou[1] | Can Cheng[1] | Fuan Niu[1] | Anpeng Zhang[1] | Bin Sun[1] | Rongjian Tu[1] | Jianing Wan[3] | Yao Li[1,4] | Yiwen Huang[1,2] | Kaizhen Xie[1,4] | Yuting Dai[1,2] | Hui Zhang[5] | Jing Han Hong[6] | Xiaohua Pan[2] | Jiaojiao Zhu[7] | Hong Zhou[7] | Zhenhua Liu[7] | Liming Cao[1] | Huangwei Chu[1]

[1]Institute of Crop Breeding and Cultivation, Shanghai Academy of Agricultural Sciences, Shanghai, China

[2]College of Agronomy, Jiangxi Agricultural University, Nanchang, Jiangxi, China

[3]Institute of Edible Fungi, Shanghai Academy of Agricultural Sciences, Shanghai, China

[4]College of Fisheries and Life, Shanghai Ocean University, Shanghai, China

[5]College of Life Science, Shanghai Normal University, Shanghai, China

[6]Cancer and Stem Cell Biology Programme, Duke-NUS Medical School, Singapore, Singapore

[7]School of Agriculture and Biology, Joint Center for Single Cell Biology, Shanghai Jiao Tong University, Shanghai, China

Correspondence
Liming Cao and Huangwei Chu, Institute of Crop Breeding and Cultivation, Shanghai Academy of Agricultural Sciences, Shanghai 201403, China.
Email: caoliming@saas.sh.cn
and chuhuangwei@saas.sh.cn

Funding information
Shanghai Technology Research Leader Program, Grant/Award Number: 18XD1424300; Shanghai Science and Technology Innovation Action Plan Project, Grant/Award Number: 21N11900100; China Postdoctoral Science Foundation, Grant/Award Number: 2021M692146; Agriculture Research System of Shanghai, Grant/Award Number: 202103; Shanghai Pujiang Program, Grant/Award Number: 20PJ1405900

Abstract

Clathrin-mediated vesicle trafficking (CMVT) is a fundamental process in all eukaryotic species, and indispensable to organism's growth and development. Recently, it has been suggested that CMVT also plays important roles in the regulation of plant immunity. However, the molecular link between CMVT and plant immunity is largely unknown. SCY1-LIKE2 (SCYL2) is evolutionally conserved among the eukaryote species. Loss-of-function of *SCYL2* in *Arabidopsis* led to severe growth defects. Here, we show that mutation of *OsSCYL2* in rice gave rise to a novel phenotype—hypersensitive response-like (HR) cell death in a light-dependent manner. Although mutants of *OsSCYL2* showed additional defects in the photosynthetic system, they exhibited enhanced resistance to bacterial pathogens. Subcellular localisation showed that OsSCYL2 localized at Golgi, trans-Golgi network and prevacuolar compartment. OsSCYL2 interacted with OsSPL28, subunit of a clathrin-associated adaptor protein that is known to regulate HR-like cell death in rice. We further showed that OsSCYL2–OsSPL28 interaction is mediated by OsCHC1. Collectively, we characterized a novel component of the CMVT pathway in the regulation of plant immunity. Our work also revealed unidentified new functions of the very conserved SCYL2. It thus may provide new breeding targets to achieve both high yield and enhanced resistance in crops.

Yao Yao and Jihua Zhou contributed equally to this study.

This is an open access article under the terms of the Creative Commons Attribution-NonCommercial-NoDerivs License, which permits use and distribution in any medium, provided the original work is properly cited, the use is non-commercial and no modifications or adaptations are made.
© 2021 The Authors. *Plant, Cell & Environment* published by John Wiley & Sons Ltd.

KEYWORDS
cell death, clathrin-mediated vesicle trafficking, disease resistance, lesion mimic mutant, *Oryza sativa*

1 | INTRODUCTION

Vesicle trafficking is a fundamental process gating intercellular communications from the cellular membrane to the cell organelles (Gu et al., 2017). The vesicles transport proteins and lipids inside a cell, which is essential for signal transduction, organelle recycling and protein renewal (Paul et al., 2014). According to the type of coated proteins, vesicle trafficking is classified as coat protein complex I (COPI)-, COPII- and clathrin-coated vesicles (CCVs) (McMahon & Mills, 2004). As a testament to its important intercellular functions, vesicle trafficking has been implicated to be vital for growth and development in yeast, animals and plants (Martinez-Ballesta et al., 2018).

In recent years, vesicle trafficking has been shown to be also involved in plant immunity and cell death. COPI-coated vesicles are implicated in retrograde cargo transportation from the Golgi apparatus to the endoplasmic reticulum (Gomez-Navarro & Miller, 2016). Depletion of either SPL35 (a ubiquitin conjugation to endoplasmic reticulum degradation domain-containing protein) or its directly interacting proteins (coatomer subunits δ-COP1 and δ-COP2) in rice, all lead to constitutive immunity activation and hypersensitive response (HR)-like cell death (Ma et al., 2019). Multivesicular bodies (MVBs) and secretory vesicles are also important for cargo transportation and plant defence. Depletion of either LRD6-6 (an AAA type ATPase i.e., required for the MVB-mediated trafficking pathway) or exocyst subunits Section 3 and EXO70 (which are involved in exocytosis) in rice, all-cause autoimmunity and HR-like cell death (Fujisaki et al., 2015; Ma et al., 2018; Zhu et al., 2016). The clathrin-mediated vesicle trafficking is an evolutionally conserved intercellular cargo transportation pathway and is recently reported to be involved in plant immunity as well. Depletion of the clathrin-associated adaptor protein complex 1, medium subunit μ1 (AP1M1) protein OsSPL28 in rice confers enhanced disease resistance and HR-like cell death (Qiao et al., 2010).

The phenotypes of the above mentioned *spl35*, *lrd6-6* and *spl28* resemble that of many lesion mimic mutants (LMMs), also termed as spotted leaf (*spl*) mutants, which have been widely used to study the relationship of plant growth and immunity (Bruggeman et al., 2015). There are about over 30 *spl* mutants that are reported in rice (Zhu et al., 2020). The underlying genes of those mutants encode for proteins involved in various genetic pathways and distinct biological processes, including heat stress transcription factors (Yamanouchi et al., 2002), U-box/armadillo repeat E3 ubiquitin ligases (Yin et al., 2000; L. R. Zeng et al., 2004), Rho GTPase-activating proteins (Akamatsu et al., 2013; J. Liu et al., 2015), hydroperoxide lyases (X. Liu et al., 2012; Tong et al., 2012), helicases (Gong *et al*., 2019), nucleus-targeted mitogen-activated protein kinases (Ueno et al., 2015), cytochrome P450 and so on (Cui et al., 2021; Fujiwara et al., 2010; Tian et al., 2020; Zheng et al., 2021). So far, only OsSPL28 has been shown to be associated with both clathrin-mediated vesicle trafficking (CMVT) and HR-like cell death (Qiao et al., 2010). Characterisation of new members connecting CMVT and plant immunity will shed insights into the understanding of the tradeoff between plant yield and immunity.

SCYL2 (SCY1-LIKE2), a member of the SCY1-like gene family, was first identified as a component of CCVs in animals (Conner & Schmid, 2005). Borner et al. (2007) showed that SCYL2 was a key regulator of development in *Xenopus tropicalis*. Others also found that SCYL2 is indispensable to neuronal function and survival in the mouse brain (Gingras et al., 2015; Pelletier, 2016). SCYL2 is conserved throughout Eukaryotes and presents as a single copy in most of the species (Jung et al., 2017). In model plant *Arabidopsis thaliana*, there are two copies of *SCYL2* (*SCYL2A* and *SCYL2B*), that function redundantly to regulate plant growth and development. Mutation of both *SCYL2A* and *SCYL2B* genes led to severe dwarfism (Jung et al., 2017). Besides the shared physiological impacts on growth and development between animals and plants, SCYL2 protein was reported to be localized to Golgi, trans-Golgi network (TGN) and vesicles in both systems (Conner & Schmid, 2005; Jung et al., 2017). So far, whether SCYL2 protein is involved in immunity are not reported.

In this study, by combining traditional map-based cloning and CRISPR-Cas9-mediated gene editing approaches (Methods), we isolated several independent mutational lines for the single *OsSCYL2* gene in rice. Different from the *SCYL2* gene mutation (which caused dwarfism) in *A. thaliana*, rice *scyl2* had only slight growth defects and the most obvious phenotype was spotted leaf since tillering stage. Our detailed phenotyping analysis showed that, although *scyl2* mutants exhibited early senescence and defects in the photosynthetic system, they were more resistant to pathogenic attacks. Subcellular localisation showed that OsSCYL2 localized at multiple organelles, including Golgi, TGN and prevacuolar compartment (PVC). Protein–protein interaction analysis further supports OsSCYL2 as a key player in the CMVT pathway by interaction with OsSPL28, subunit of a clathrin-associated adaptor protein that is known to regulate HR-like cell death in rice. We further showed that OsSCYL2–OsSPL28 interaction was mediated by OsCHC1, a heavy chain of clathrin-coated on vesicles. Taken together, our work revealed unidentified functions of the evolutionally conserved SCYL2 by modulating plant immunity through the CMVT-mediated pathway in rice. It thus will add insights into our understanding of the balance between yield and defence output in crop breeding.

2 | MATERIALS AND METHODS

2.1 | Plant materials and growth conditions

Rice cultivar *japonica* cv. Xiushui 134 (XS134) was used as wild type (WT) for phenotypic characterisation and genetic transformation assay in this study. Transgenic-free plants were grown in the paddy field at the Zhuanghang Experimental Station of the Institute of Shanghai Academy of Agricultural Sciences. Transgenic or CRISPR-Cas9 plants were grown in Baihe Transgenic Experimental Station of the Institute of Shanghai Academy of Agricultural Sciences.

2.2 | Forward genetics for *OsSCYL2* isolation

scyl2-1 mutant was isolated from M_2 population seeds of XS134 treated by ethyl methanesulfonate. For genetic analysis, *scyl2-1* was crossed with the WT. F_1 plants exhibited a similar phenotype as the WT, while the F_2 population yielded a segregation of 261 normal and 106 mutant plants (3:1, $\chi^2 = 1.36 < \chi^2_{0.05} = 3.84$), indicating that *scyl2-1* is a recessive mutant controlled by a single gene locus. To genetically map the locus responsible for the mutant phenotype, *scyl2-1* was crossed with an *indica* rice variety (9311). A total of 87 plants exhibiting the *scyl2-1* mutant phenotype were selected from F_2 progeny for genetic mapping. The *scyl2-1* locus was initially localized within the region between insertion–deletion (Indel) marker ID2 and ID5 on chromosome 1 (Figure 1a). To refine the genetic mapping, an additional 482 F_2 mutant individuals derived from the same cross and two newly developed Indel markers (primers listed in Table S1) were used. The *scyl2-1* causing locus was finally delimited to an 18 kb region between ID3 and ID4 (Figure 1b). Only one open reading frame (ORF, *LOC_Os01g42950*) was annotated in this region (Figure 1c) according to the database in Rice Genome Annotation Project (http://rice.plantbiology.msu.edu/). Sequencing and comparison of *LOC_Os01g42950* cloned from WT and *scyl2-1* revealed that a 12 bp-deletion was occurred in the fourth exon of *OsSCYL2* in the mutant (Figure 1d).

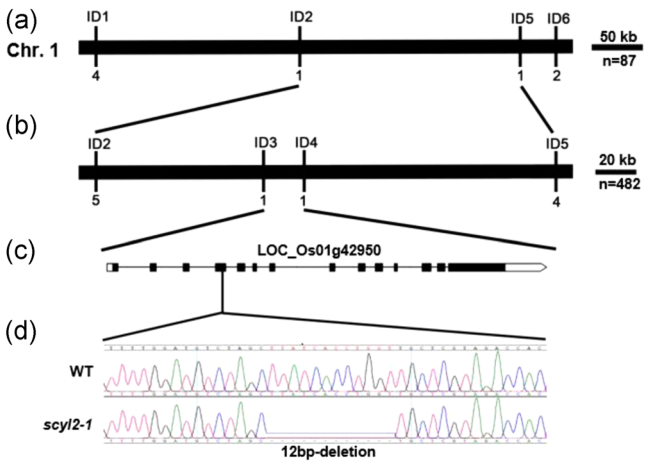

FIGURE 1 Map-based cloning of *OsSCYL2* gene. (a) The *scyl2-1* mutation was located on chromosome 1 between Indel markers ID2 and ID5. (b) The *scyl2-1* mutation was delimited to an interval about 18 kb between Indel markers ID3 and ID4 using 482 mutant F_2 individuals. (c) Only 1 open reading frame, LOC_Os01g42950 (*OsSCYL2*) which has 14 exons and 13 introns, was predicted in the ID3–ID4 interval. Exons and introns are indicated by black rectangles and black lines, respectively. (d) A 12 bp-deletion in the fourth exon of *LOC_Os01g42950* (*OsSCYL2*) was identified in the *scyl2-1*

To verify whether the 12 bp-deletion in *OsSCYL2* was responsible for the *scyl2-1* mutant phenotype, we conducted a genetic complementation assay. The maize ubiquitin promoter and *OsSCYL2* complementary DNA (cDNA) were amplified, respectively, and fused into binary pCAMBIA 1301 vector between restriction sites SacI and BstEII using Trelief™ SoSoo Cloning Kit (Tsingke). The primers were listed in Table S2. The resultant vector was introduced into *scyl2* mutant by *Agrobacterium tumefaciens*-mediated (EHA105 strain) transformation. Of 11 T_0 plants, 8 were positive transformants and all of them exhibited the same phenotypes as the WT (Figure S1a,b).

2.3 | CRISPR-Cas9-mediated *OsSCYL2* knock out

The CRISPR-Cas9 guide-RNA (gRNA) targeted sequence of *OsSCYL2* gene was selected using the CRISPR Primer Designer program (Figure S2a; Yan et al., 2015). A previously described CRISPR-Cas9 vector (H. Zhang et al., 2014) engineered with gRNA targeted elements was constructed and introduced into XS134 by *A. tumefaciens*-mediated transformation. Three independent knockout lines (*scyl2-2*, *scyl2-3* and *scyl2-4*) were obtained and they all showed the same phenotype as *scyl2-1* (Figure 2b,c).

2.4 | Transient assays in *Nicotiana benthamiana*

For subcellular localisation analysis, coding sequences (CDS) of *OsSCYL2* and eYFP were inserted into the *Nco*I and *Bst*EII sites of binary pCAMBIA 1301 vector using Trelief™ SoSoo Cloning Kit (Tsingke). *OsSCYL2:YFP* vector and various cellular organelle marker were transformed into GV3101 strains containing the P19 gene-silencing suppressor protein. For BiFC assay, full-length cDNA of *OsSPL28* and *OsSCYL2* were cloned into pXY104-cYFP plasmid, respectively, and full-length cDNA of *OsSPL28* and *OsCHC1* were cloned into pXY106-nYFP, respectively. Complementary recombinant constructs were co-transformed to detect protein–protein interactions. *Agrobacterium*-mediated infiltration of tobacco leaf epidermal cells was performed using a syringe. For cotransformation the bacteria were mixed in appropriate volumes of infiltration buffer before injection into the leaves. Fluorescent signals were detected using laser confocal scanning microscopy (ZEISS Microscopy LSM700) 4–5 days after infiltration.

For the split-luciferase assay, full-length cDNA of *OsCHC1* and *OsSCYL2* were cloned into pCAMBIA1300-cLUC plasmid, respectively.

Meanwhile, full-length cDNA of *OsSPL28* and *OsSCYL2* were cloned into pCAMBIA1300-nLUC, respectively. Complementary recombinant constructs were co-transformed into tobacco leaf epidermal cells as described in above and grown in the dark for 40 h. The leaves were then sprayed with 5 mM luciferin and kept in the dark for 10 min to quench the fluorescence. Images were captured by a cooling CCD imaging apparatus (Tanon 5200).

2.5 | Quantitative real-time polymerase chain reaction analysis

For *OsSCYL2* expression pattern analysis, root, stem, leaf, leaf sheath and panicle samples were collected from the WT plant at the flowering stage. For defence response and reactive oxygen species (ROS) scavenge related gene expression analysis, the second fully-expanded leaf were collected from WT and *scyl2* mutants at tillering stage. Total RNA was extracted from the samples using RNAprep Pure Plant Kit (Cat No. DP441; Tiangen Biotech). cDNA was prepared from total RNA using a reverse transcription kit (Cat No. FSQ-301; Toyobo). The rice *ACTIN* gene was used as an internal control. The $2^{-\Delta\Delta C_t}$ was used to determine relative expression levels of gene expression. All primers used for quantitative real-time polymerase chain reaction (qRT-PCR) analysis are listed in Table S3.

2.6 | Construction of *OsSCYL2pro::β-Glucuronidase* lines

The *OsSCYL2* promoter region (2372 bp) was amplified from WT genomic DNA and cloned into pCAMBIA1301 between *Hin*dIII and *Nco*I sites using Trelief™ SoSoo Cloning Kit (Tsingke). *OsSCYL2pro::β-Glucuronidase (GUS)* was introduced into WT XS134 by *A. tumefaciens*-mediated transformation. Four independent lines were randomly selected for GUS staining as described previously (Chu et al., 2013). Tissues were treated with GUS solution at 37°C for 8 h, and then were cleaned using 95% alcohol at 65°C. All lines showed similar GUS staining patterns in accordance with the expression pattern observed by RT-qPCR analysis. The primers and oligos used for the above vectors constructed are listed in Table S2.

2.7 | Histochemical assays

Fresh flag leaves of WT and *scyl2-1* at the flowering stage were used in the histochemical experiment. Trypan blue staining was performed as described by Yin et al. (2000). Briefly, leaves were submerged in trypan blue solution (0.25% trypan blue, 25% lactic acid, 23% water-saturated phenol, 25% glycerol in ddH_2O), infiltrated at 70°C for 10 min, and then heated in boiling water for 2 min and left to stain at room temperature overnight. Trypan blue solution was replaced with chloral hydrate solution (25 g in 10 ml of H_2O) for destaining. After multiple exchanges of chloral hydrate solution for 3 days, samples were equilibrated with 70% glycerol, and then used for photograph. 3,3′-Diaminobenzidine (DAB) staining assay for H_2O_2 detection was performed as described by Qiao et al. (2010). Briefly, leaf samples were vacuum-infiltrated (three times of 10 min each) in DAB staining solution containing 1 mg/ml DAB and 10 mM 2-(N-Morpholino) ethanesulfonic acid (pH 6.5), and then stained at room temperature for 18 h in the dark. The reactions were stopped by transfer to 90% ethanol at 70°C until chlorophyll was completely removed. The cleared leaves were examined and photographed in 70% glycerol. Chlorophyll and carotenoid content were measured as described previously (Wellburn, 1994). Malondialdehyde (MDA) and soluble protein content, superoxide dismutase (SOD) and peroxidase (POD) activities in leaves, were measured using MDA, soluble protein, SOD and POD assays kit (COMIN Biotechnology), respectively, according to the manufacturer's instruction. Net photosynthetic rate was measured using a plant photosynthetic meter (Tuopu) according to the manufacturer's instruction.

2.8 | Transmission electron microscopy

The second leaf from plants at tillering stage grown under the normal field condition were fixed in 0.2 N sodium phosphate buffer (pH 7.0) containing 3% (wt/vol) paraformaldehyde and 0.25% glutaraldehyde, and then postfixed phosphate-buffered saline (pH 7.2) containing 2% OsO_4. Samples were embedded in acrylic resin after ethanol dehydration. A total of 50 nm ultra-thin sections were double-stained with 2% (wt/vol) uranyl acetate and 2.6% (wt/vol) lead citrate aqueous solution. Images were taken using a JEM-1230 transmission electron microscope (JEOL) at 80 kV.

2.9 | Yeast two-hybrid assay

Full-length cDNA of *OsCHC1*, *OsSPL28*, *OsVTI11* and *OsVTI12* were cloned into pGADT7 as prey, respectively. Full-length cDNA of *OsSPL28* and *OsSCYL2* were cloned into pGBKT7 as bait, respectively. For yeast two-hybrid assay, the prey and bait vector were cotransformed into yeast AH109 competent cells. Each transformed cell was first incubated on SD/-Leu-Trp solid media (Clontech) and then transferred to restrictive media SD/-Leu-Trp-His-Ade and cultured at 30°C for 4 days.

2.10 | RNA-seq and Gene Ontology enrichment analysis

For *scyl2-1* transcriptomic analysis, the second fully-expanded leaves of three individual WT and three individual *scyl2-1* plant, respectively, at the tillering stage were collected for extracting total RNA.

A total of six RNA samples were used for RNA-seq analysis. RNA-seq library preparation and sequencing were performed by NOVELBIO.

The differentially expressed genes were identified by using Algorithm DEseq. 2 (Love et al., 2014). The Benjamini–Hochberg model was used to calculate false discovery rate (FDR) (Benjamini & Hochberg, 1995). The significant enriched Gene Ontology (GO) pathways were selected by using Fisher's extract test, and the threshold of significance was defined by $p \leq 0.01$ (Draghici et al., 2007).

3 | RESULTS

3.1 | *scyl2* is a newly identified LMM in rice

scyl2 mutant was initially identified through a map-based cloning approach (Figure 1) and named as *scyl2-1*. Sequencing analysis revealed that a 12 bp-deletion occurred in the fourth exon of *OsSCYL2* (*LOC_Os01g42950*) gene in *scyl2-1* (Figures 1d and 2a). The genetic analysis further indicated that *scyl2-1* is a recessive mutant solely controlled by mutation of the *OsSCYL2* gene in rice (Method). There were no significant growth differences between WT and *scyl2-1* leaves at the early growth stage under normal field growth conditions. Until the tillering stage, small reddish-brown necrotic spots appeared on the newly grown leaves of *scyl2-1* mutant plants and gradually spread to the whole leaves. Meanwhile, *scyl2-1* leaves started to initiate early senescence from the leaf apex (Figure 2b,c). At the maturation stage, the lesion phenotype of *scyl2-1* leaves became more severe, showing a dark brown colour and appeared on the leaf sheath and grain hulls (Figures 2c,d and 3a).

It has been shown that lesion formation in most of the LMMs is light-dependent (Rao et al., 2020; L. R. Zeng et al., 2004; Y. Zhang et al., 2019). To examine the response of *scyl2-1* mutant to light, newly emerged leaves of *scyl2-1* and WT were covered with 2–3 cm width aluminium foil for 7 days. This experiment revealed that the leaf area of *scyl2-1* without light exposure was as normal as WT without lesion phenotype (Figure 2e), indicating that the lesion mimic formation in *scyl2-1* is light-dependent.

In addition to those HR-like lesion phenotypes, *scyl2-1* also exhibited alterations in several important agronomic traits, including plant height, grain number per panicle, seed setting rate, grain length, grain width, grain thickness, and 1000-grain weight. Notably, no significant differences were found for tiller number and panicle length between WT and *scyl2-1* plants (Figure 3a–j).

To verify the lesion mimic phenotype was indeed caused by mutation of the *OsSCYL2* gene, two approaches were applied.

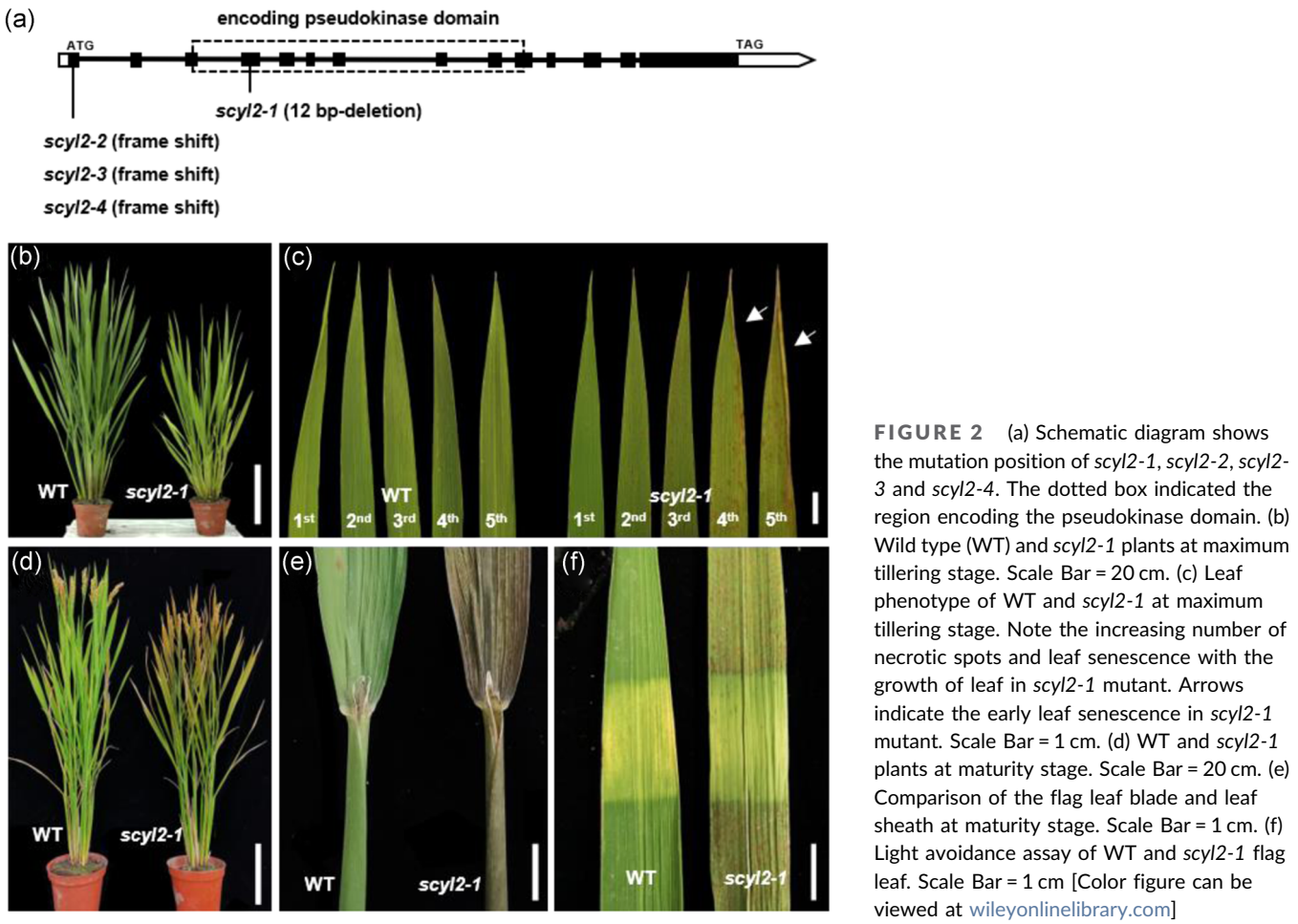

FIGURE 2 (a) Schematic diagram shows the mutation position of *scyl2-1*, *scyl2-2*, *scyl2-3* and *scyl2-4*. The dotted box indicated the region encoding the pseudokinase domain. (b) Wild type (WT) and *scyl2-1* plants at maximum tillering stage. Scale Bar = 20 cm. (c) Leaf phenotype of WT and *scyl2-1* at maximum tillering stage. Note the increasing number of necrotic spots and leaf senescence with the growth of leaf in *scyl2-1* mutant. Arrows indicate the early leaf senescence in *scyl2-1* mutant. Scale Bar = 1 cm. (d) WT and *scyl2-1* plants at maturity stage. Scale Bar = 20 cm. (e) Comparison of the flag leaf blade and leaf sheath at maturity stage. Scale Bar = 1 cm. (f) Light avoidance assay of WT and *scyl2-1* flag leaf. Scale Bar = 1 cm [Color figure can be viewed at wileyonlinelibrary.com]

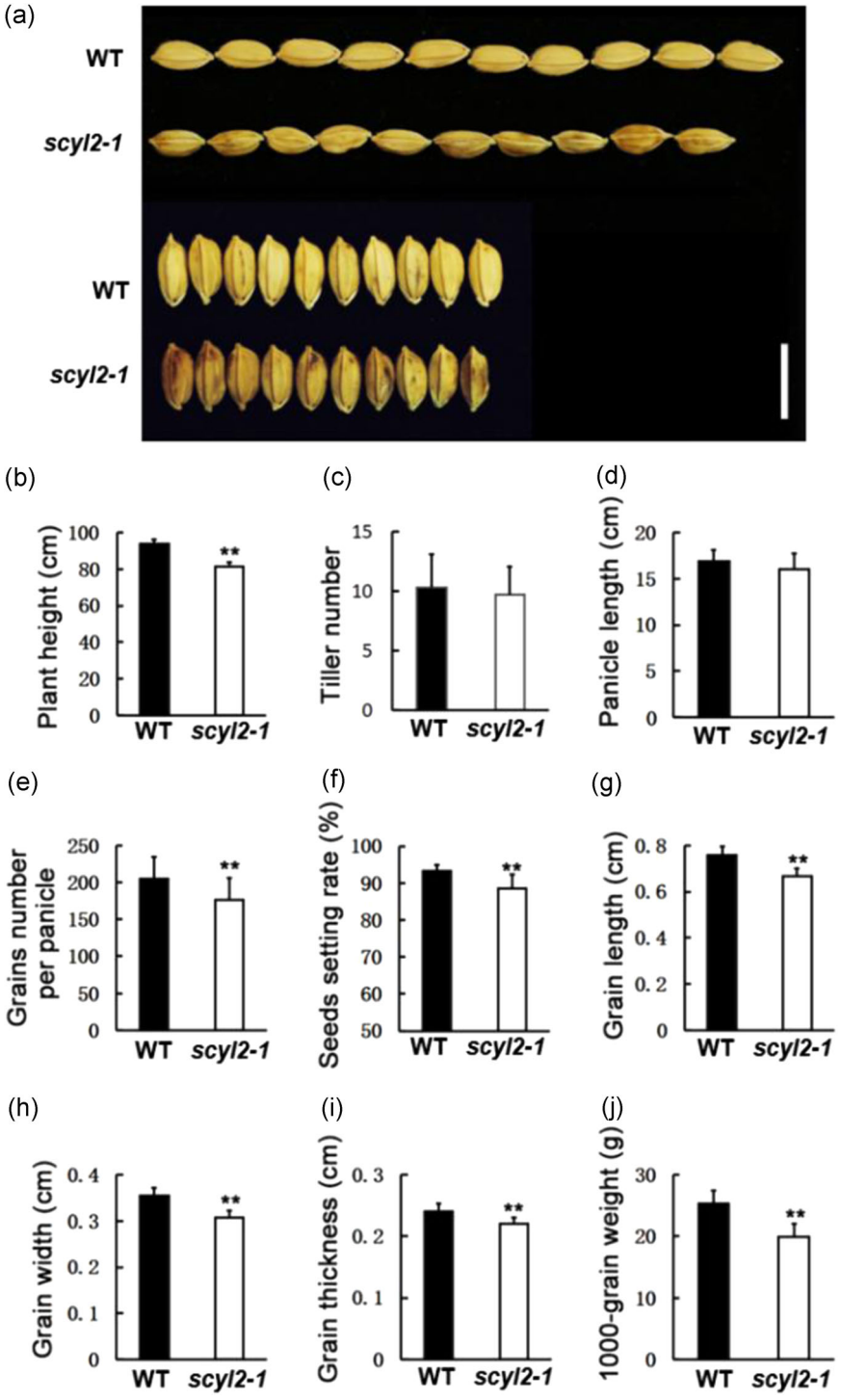

FIGURE 3 *scyl2-1* exhibited alterations in several important agronomic traits. (a) Grain phenotypes of wild type (WT) and scyl2-1. The grain size of *scyl2-1* was smaller as compared WT, and lesion mimic phenotype could be observed on the surface of grain hulls of WT and *scyl2-1*. Scale Bar = 1 cm. Plant height of WT and *scyl2-1* at the maturation stage. (c) Tiller number of WT and *scyl2-1*.(d) Panicle length of WT and *scyl2-1*. (e) Grain number per panicle of WT and *scyl2-1*. (f) Seed setting rate of WT and *scyl2-1*. (g) Grain length of WT and *scyl2-1*. (h) Grain width of WT and *scyl2-1*. (i) Grain thickness of WT and *scyl2-1*. (j) 1000-Grain weight of WT and *scyl2-1*. Error bars indicate standard deviation of twenty biological replicates, $^{**}p < 0.01$ [Color figure can be viewed at wileyonlinelibrary.com]

Firstly, we cloned the full-length CDS of *OsSCYL2* and introduced into the *scyl2-1* mutant driven by maize *Ubiquitin1* promoter by *A. tumefaciens*-mediated transformation. Of 11 T0 plants, 8 were positive transformants, and all of them exhibited the same phenotypes as the WT (Figure S1a,b). Secondly, we disrupted the *OsSCYL2* using CRISPR/Cas9 technology in WT (Figure S2a). Three independent knockout mutants, designated as *scyl2-2* to *scyl2-4*, respectively, were obtained (Figure S2b). All of these knockout mutants showed lesion mimic phenotype as observed in the *scyl2-1* (Figure S2c). These CRISPR/Cas9 edited mutants had strong genetic mutations (e.g., frame-shift since the first exon; Figure 2a,b), suggesting that the four amino acids in the pseudokinase domain (causal mutation in *scyl2-1*) are essential for OsSCYL2's biological function (Figure 2a). Together, our results demonstrate that *scyl2-1* is a newly identified LMM in rice.

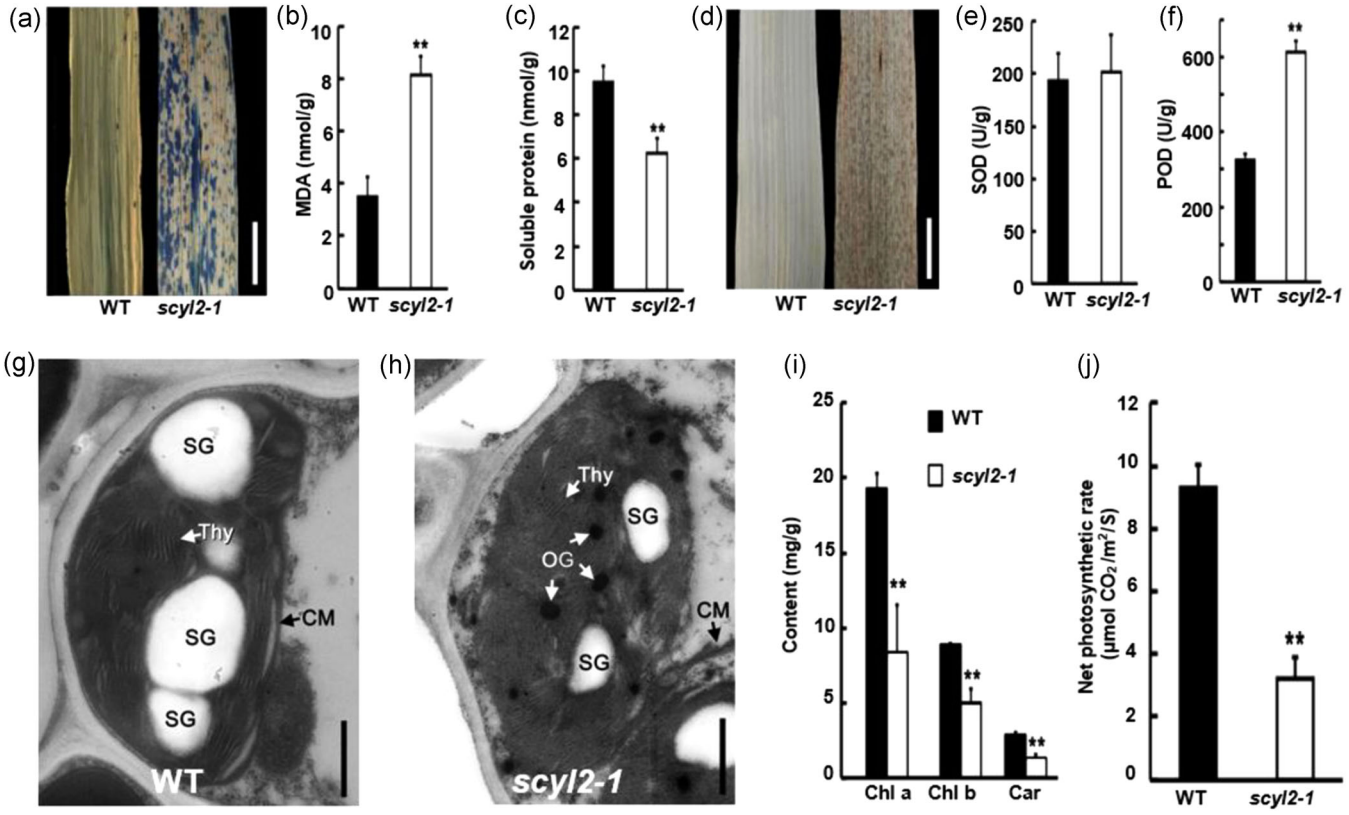

FIGURE 4 Mutation of *OsSCYL2* led to cell death, ROS accumulation, and abnormal chloroplast morphology and activities. (a) Dead cells were detected by trypan blue staining. Scale Bar = 1 cm. (b) MDA content in the WT and *scyl2-1* flag leaves. Error bars indicate the standard deviation of three biological replicates, $^{**}p < 0.01$. (c) Soluble protein in the WT and *scyl2-1* flag leaves. Error bars indicate the standard deviation of three biological replicates, $^{**}p < 0.01$. (d) In situ detection of H_2O_2 in leaves by DAB staining. Scale Bar = 1 cm. (e) The enzymatic activities of SOD in the WT and *scyl2-1* flag leaves. Error bars indicate the standard deviation of three biological replicates. (f) The enzymatic activities of POD in the WT and *scyl2-1* flag leaves. Error bars indicate the standard deviation of three biological replicates, $^{**}p < 0.01$. (g, h) Chloroplast ultrastructure in WT (g) and *scyl2-1*. (h) Flag leaves at a flowering stage when the lesion symptom was observed in *scyl2-1*. Scale Bar = 1 μm. (i) Chlorophyll content in the flag leaves of WT and *scyl2-1* plants. Error bars indicate the standard deviation of three biological replicates, $^{**}p < 0.01$. (j) Net photosynthetic rate in the WT and *scyl2-1* flag leaves. Error bars indicate standard deviation of eight biological replicates, $^{**}p < 0.01$. Car, carotenoid; Chl a, chlorophyll a; Chl b, chlorophyll b; CM, chloroplast membrane; DAB, 3,3′-diaminobenzidine; MDA, malondialdehyde; OG, osmiophilic globules; POD, peroxidase; SG, starch granule; SOD, superoxide dismutase; Thy, thylakoid lamellae; WT, wild type [Color figure can be viewed at wileyonlinelibrary.com]

3.2 | Mutation of *OsSCYL2* caused cell death and ROS accumulation

To understand the cause of lesion formation in *scyl2-1* leaves, we carried out trypan blue staining analysis, a traditional assay used for detecting cell death and irreversible membrane damage (Dietrich et al., 1994). We observed a mass of deep blue spots at lesion sites in the *scyl2-1* mutant, suggesting that cell death has likely happened in the lesion area (Figure 4a). Next, we compared the content of MDA and soluble protein (cell membrane damage indicators) between WT and *scyl2-1* mutant plants. The MDA content was significantly increased, with a concomitant decrease of soluble protein content in *scyl2-1* as compared with WT (Figure 4b,c). These experiments indicated that the HR-like cell death indeed occurred in *scyl2-1* leaves.

It has been reported that HR-like cell death is strongly associated with the accumulation of ROS (Coll et al., 2011). We, therefore, examined the H_2O_2 production (one of the main types of ROS) in WT and *scyl2-1* using DAB staining. This assay revealed that H_2O_2 production was only associated with lesion formation in cleared *scyl2-1* leaves, but not in cleared WT leaves (Figure 4d). We also examined the gene expressions of several ROS scavenging related genes, including *SOD*, catalase (*CAT*) and *POD* which are usually activated to eliminate the elevated ROS under oxidative stresses (Miller et al., 2010). The qRT-PCR results indicated that the expression of *POD* in *scyl2-1* was more than 30-fold higher than in WT, although the expressions of both *SOD* and *CAT* in the *scyl2-1* were not clearly changed (Figure S3). In agreement with this, POD activities were significantly increased in *scyl2-1* mutant compared to WT, whereas SOD activities in *scyl2-1* were similar to WT (Figure 4e,f).

3.3 | Mutation of *OsSCYL2* led to abnormal chloroplast morphology and activities

It has been reported that the lesion symptom of many *spl* mutants is light-dependent and those mutants usually had defects in the chloroplast activity (Bruggeman et al., 2015). It was also suggested that damaged chloroplast membranes could trigger bursts of ROS and further induce cell death (Zurbriggen et al., 2009). Therefore, we speculated that the HR-like cell death observed in *scyl2-1* could be a consequence of chloroplast structural perturbations. We examined the ultrastructure of chloroplasts using transmission electron microscopy in the second leaf at tillering stage, when the lesion just began to form (Figure 2c). The chloroplast in WT leaves were well developed and contained rich and neatly stacked thylakoid lamellae, wrapped in the intact chloroplast membrane (Figures 4g and S4a). In contrast, the thylakoids were smaller with disorganized lamellae, and the chloroplast membrane was likely degraded in *scyl2-1* (Figures 4h and S4b). Moreover, the increased size and number of osmiophilic globules, which is generally observed during chloroplast senescence (Hopkins et al., 2007), appeared in the stroma of *scyl2-1* mutant (Figures 4h and S4b). In line with this, the levels of chlorophylls (a & b) and carotenoid were significantly reduced in flag leaves of *scyl2-1* mutants in comparison to WT (Figure 4i). In addition, the net photosynthetic rate of *scyl2-1* was significantly slower than that of WT (Figure 4j). Altogether, our results revealed that mutation of *OsSCYL2* caused defects in both chloroplast morphology and activities.

3.4 | *scyl2-1* showed constitutively activated defence responses

It has been reported that most of the *spl* mutants exhibited enhanced pathogen resistance (Ma et al., 2019). We thus inoculated WT and *scyl2-1* plant with three rice disease-causing bacterial cells, P6, P7 and XOO4 (*Xanthomonas oryzae* pv. *oryzae*), by the leaf-clipping method at the tillering stage (Rao et al., 2020). The *scyl2-1* mutant exhibited significantly ($p \leq 0.01$) enhanced resistance to all three bacterial isolates compared to WT (Figure 5a,b). Enhanced diseases of LMM are often associated with elevated expression levels of genes from different defence response pathways (S. Wang et al., 2017; Z. Wang et al., 2015). Therefore, we quantified and compared 14 defence response genes either involved in SA- or JA-signalling pathways between WT and *scyl2-1* mutant by qRT-PCR analysis. Of that, four genes

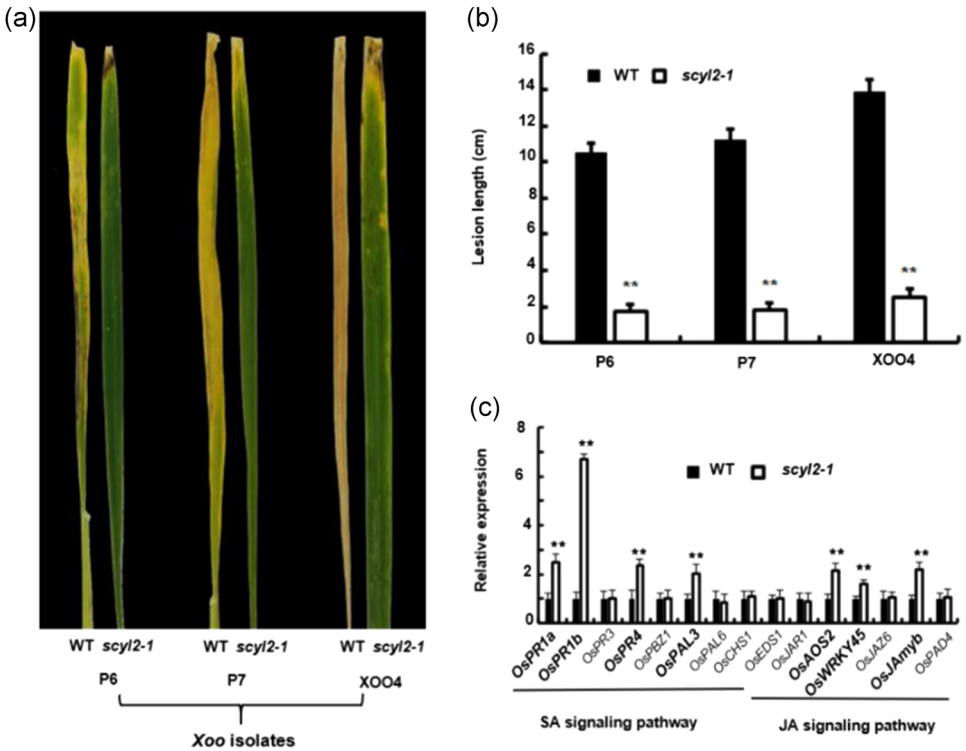

FIGURE 5 Defence responses are constitutively activated in the *scyl2-1* mutant. (a) The leaves of the WT and *scyl2-1* mutant 2 weeks after inoculation with *Xanthomonas oryzae* pv. *Oryzae* (Xoo) isolates P6, P7 and XOO4, respectively. (b) Lesion length in the WT and *scyl2-1* 2 weeks after inoculation with Xoo isolates P6, P7 and XOO4, respectively. Error bars indicate standard deviation of 15 biological replicates, $^{**}p < 0.01$. (c) Comparison of expression levels of defence response genes involved in SA- and JA-signalling pathway between the WT and *scyl2-1* using the qRT-PCR assay. The second fully-expanded leaves at the tillering stage were collected for analysis. Error bars indicate the standard deviation of three biological replicates, $^{**}p < 0.01$. qRT-PCR, quantitative real-time polymerase chain reaction; WT, wild type [Color figure can be viewed at wileyonlinelibrary.com]

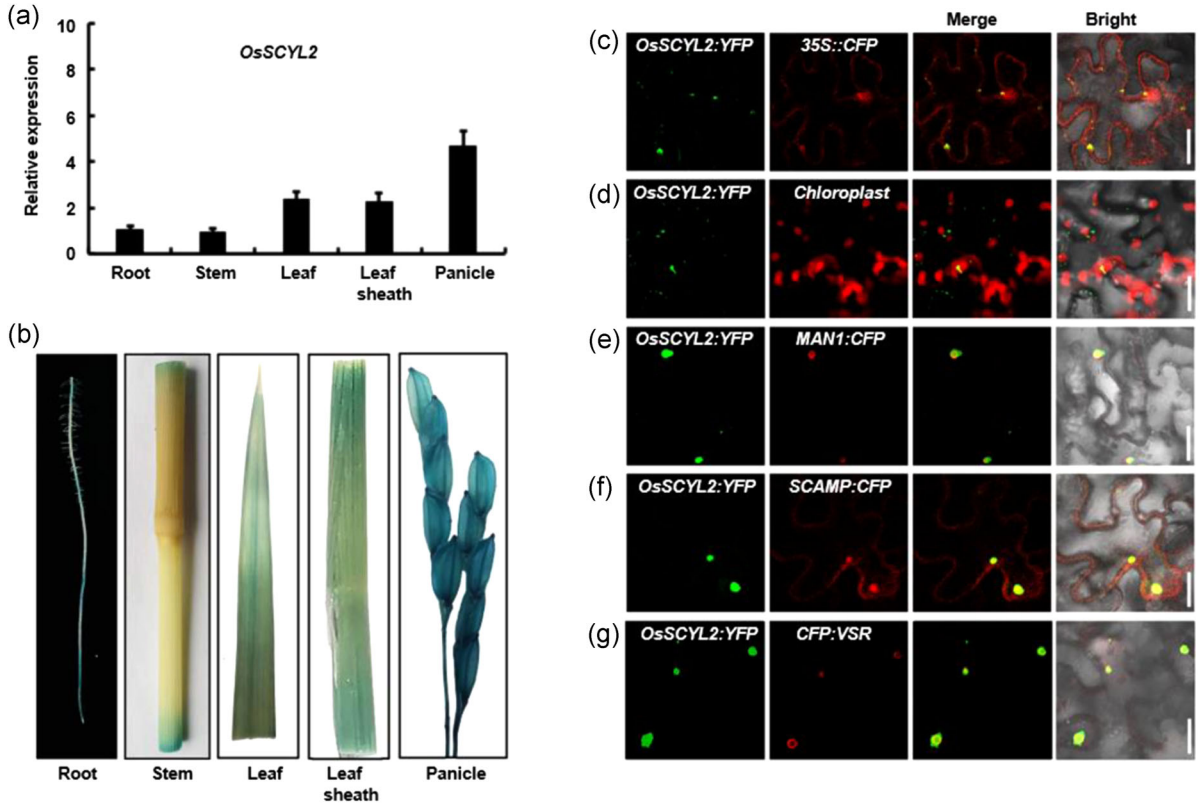

FIGURE 6 Expression pattern of *OsSCYL2* and subcellular localisation of OsSCYL2. (a) qRT-PCR analysis of *OsSCYL2* expression in various tissues. Tissues were from plants at the heading stage. Error bars indicate the standard deviation of three biological replicates. (b) Gus staining of *SPL38pro:GUS* transgenic plants at heading stage. (c) Tobacco leaf epidermal cells expressing *OsSCYL2:YFP* (green) and *35S::CFP* (red). Scale Bar = 20 μm. (d) Tobacco leaf epidermal cells expressing *OsSCYL2:YFP* (green). Chloroplasts in the cell were visualized by chlorophyll autofluorescence (red). Scale Bar = 20μm. (e–g) Tobacco leaf epidermal cells were cotransformed with *OsSCYL2:YFP* and the subcellular organelles markers for Golgi (e), TGN (f) and PVC (g). Scale Bars = 20 μm. qRT-PCR, quantitative real-time polymerase chain reaction
[Color figure can be viewed at wileyonlinelibrary.com]

(*OsPR1a*, *OsPR1b*, *OsPR4* and *OsPAL3*) in the SA-signalling pathway and three genes (*OsAOS2*, *OsWRKY45* and *OsJAmyb*) in the JA-signalling pathway were significantly elevated in *scyl2-1* than those of WT (Figure 5c). These results suggested that *scyl2-1* had gained enhanced resistance to diseases, most likely due to constitutive activation of the expressions of defence response genes, though whether JA or SA is directly involved in the activation of those responsive genes needs further careful investigations. The enhanced defence response (Figure 5a–c) accompanied by the alteration in agronomic traits (Figure 3a–j) observed in *scyl2-1*, suggest that the *OsSCYL2* gene plays a pivotal role in balancing the plant growth/development and defence.

3.5 | OsSCYL2 localized at the Golgi, TGN and PVC

We first carried out qRT-PCR analysis to reveal the gene expression pattern of the *OsSCYL2* gene in various rice organs. Gene expression of *OsSCYL2* was broadly detected, including in root, stem, leaf, leaf sheath and panicle, with the highest expression observed in the panicle (Figure 6a). In agreement with this, plants carrying *OsSCYL2* promoter fused with GUS reporter gene showed GUS staining similar to the pattern observed by qRT-PCR analysis (Figure 6b). As mutation in *OsSCYL2* showing enhanced resistance to blight pathogens (Figure 5a,b), we performed a time course qRT-PCR analysis of *OsSCYL2* expression levels in flag leaves of WT plant with *Xoo* isolates PXO99A. The expression level of *OsSCYL2* was significantly suppressed after inoculation at all time points after infection (Figure S5), suggesting a negative role of OsSCYL2 in plant immunity. To gain knowledge about OsSCYL2 protein localisation at the subcellular level, we created *OsSCYL2:YFP* fusion proteins under the control of a constitutive CaMV 35S promoter and transiently expressed the proteins in *Nicotiana benthamiana* leaf epidermal cells. The *OsSCYL2:YFP* fusion proteins were predominantly localized in punctate or vesicular structure compartments, which are distinct from free CFP or chloroplast autofluorescent (Figure 6c,d). In addition, the *OsSCYL2:YFP* signal overlapped with fluorescent markers targeted to specific subcellular compartments, including Golgi, TGN and PVC (Figure 6e–g). In *Arabidopsis*, orthologs of SCYL2 proteins (SCYL2A and SCYL2B) are also localized at these vesicles trafficking-related organelles (Jung et al., 2017),

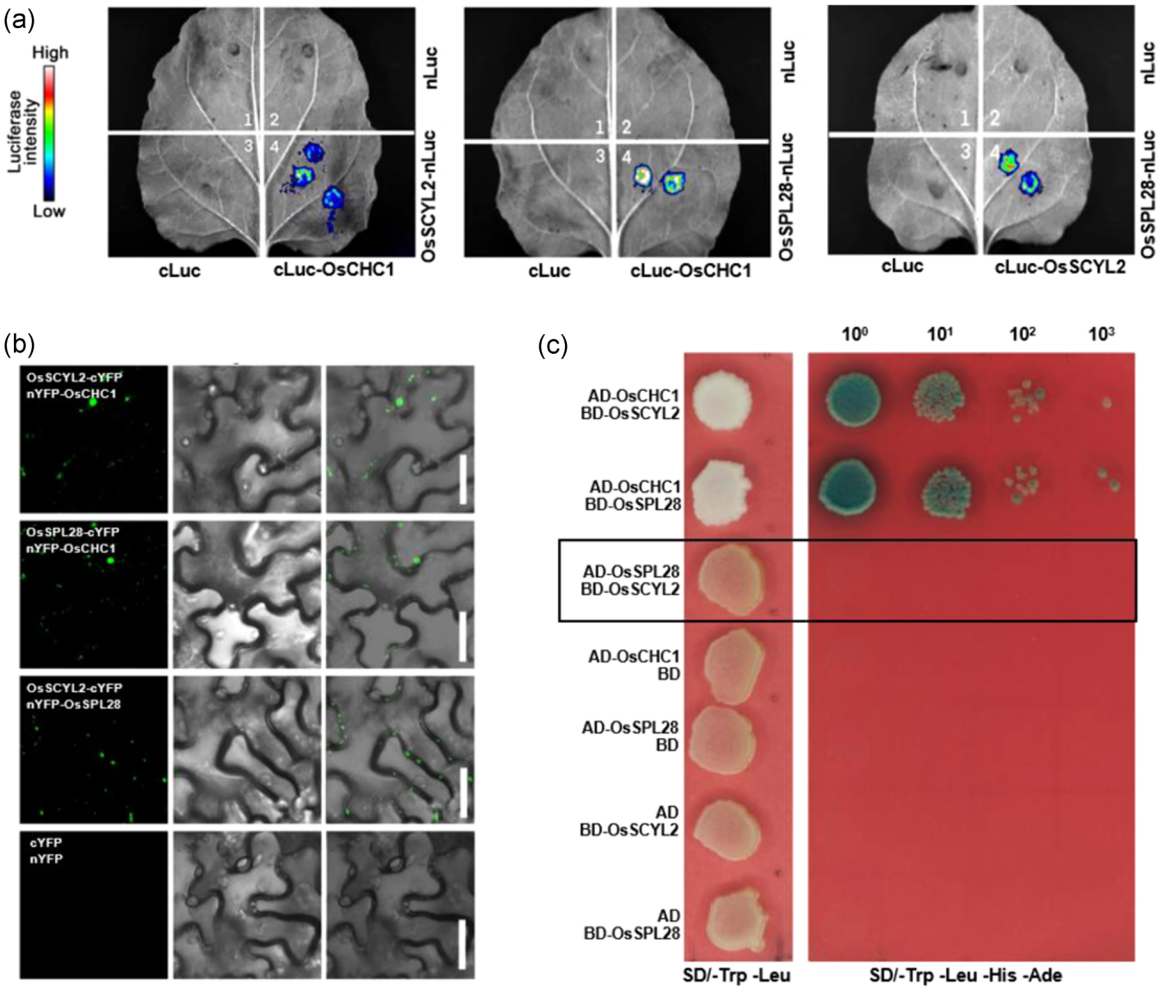

FIGURE 7 OsSCYL2 interact with OsSPL28 via OsCHC1. (a) Pairwise interaction of OsSCYL2, OsSPL28 and OsCHC1 using the split-luciferase assays in tobacco leaf. (b) Pairwise interaction of OsSCYL2, OsSPL28 and OsCHC1 using the BiFC assays in tobacco leaf epidermal cells. Scale Bars = 25 μm. (c) OsSCYL2 and OsSPL28 interact with OsCHC1 in a yeast two-hybrid assay. It is noted that OsSPL28 and OsSCYL2 do not interact with each other in yeast two-hybrid (indicated by black box). AD, activating domain; BD, DNA-binding domain; BiFC, bimolecular fluorescence complementation; cYFP, C-terminal yellow fluorescent protein; nYFP, N-terminal yellow fluorescent protein; SD, synthetic defined medium [Color figure can be viewed at wileyonlinelibrary.com]

suggesting that SCYL2 has conserved subcellular localisation between rice and *Arabidopsis*, although its biological functions might be divergent between monocots and dicots. Our results showed that transcription of *OsSCYL2* was suppressed after striking by *Xoo*, yet whether pathogen or ROS infection will affect the cellular behaviour of OsSCYL2 needs to be investigated using stably transformed lines.

3.6 | OsSCYL2 interacted with OsSPL28 likely via OsCHC1 in rice

In *A. thaliana*, SCYL2 interacts with various CCV components, such as CHC1 (heavy chain of clathrin) and two Soluble NSF Attachment Protein Receptors (SNAREs): Vesicle Transport through t-SNARE Interaction11 (VAT11) and VAT12 (Jung et al., 2017). To determine the interactive partners of OsSCYL2 in rice, we carried out a split-luciferase assay and split YFP-based bimolecular fluorescence complementation (BiFC) in a transiently expressed *N. benthamiana* system. Our analysis revealed that OsSCYL2 could interact with OsCHC1 (*LOC_Os11g01380*) (M. Zeng et al., 2013), OsVTI11 (*LOC_Os01g37980*) and OsVTI12 (*LOC_Os01g51120*) (Sutter et al., 2006), respectively (Figures 7a,b and S6a). OsSPL28 (clathrin-related adaptor) was previously reported to be directly associated with both CMVT and plant cell death in rice. Mutation in the *OsSPL28* gene in rice also led to a significant decrease in chlorophyll content, elevated ROS production and enhanced disease resistance (Qiao et al., 2010). We thus included OsSCYL2 and OsSPL28 proteins in our BiFC and split-luciferase assays. Our results indicated that

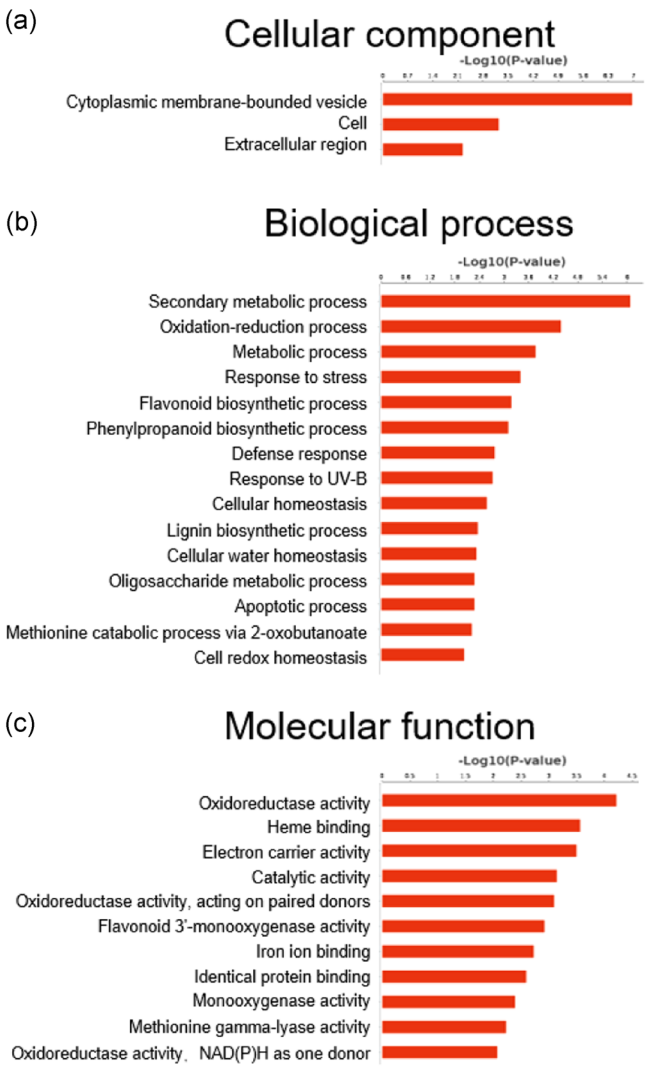

FIGURE 8 Gene Ontology functional enrichment analysis. (a) Cellular component category. (b)Biological process category. (c) Molecular function category [Color figure can be viewed at wileyonlinelibrary.com]

they indeed could interact in both BiFC or split-luciferase assays (Figure 7a,b). Since mutations of *OsSCYL2* and *OsSPL28* in rice confer similar phenotypes (Qiao et al., 2010), we infer that OsSCYL2 could interact with OsSPL28 to regulate plant immunity in rice. To determine if OsSCYL2 could directly interact with OsSPL28, we conducted yeast two-hybrid assays. We could not detect any interaction of OsSCYL2 with OsSPL28 (or OsVTI11 and OsVTI12) in yeast two-hybrid assays, but there was clear evidence supporting the interaction of OsCHC1 with either OsSCYL2 or OsSPL28 (Figures 7c and 6b). Altogether, we thus inferred that the interaction between OsSCYL2 and OsSPL28 is indirect, and the heavy chain of clathrin protein OsCHC1 provides an anchoring point for interactions among OsSCYL2, OsSPL28 and v-SNARE proteins (OsVTI11 and OsVTI12) and they likely form a functional module to simultaneously regulate plant immunity in rice.

3.7 | Insights of OsSCYL2's function in the regulation of rice immunity by RNA-sequencing

To decipher a possible OsSCYL2 regulatory network, we performed RNA-sequencing on WT and *scyl2-1* leaves at tillering stage, when lesion phenotypes started to emerge. A total of 48 downregulated and 170 upregulated DEGs were identified (FDR < 0.05; $\log_2$FC <−1 or >1; Table S4). GO analysis revealed that the 'cytoplasmic membrane-bounded vesicle' was the most significantly enriched GO term in the cellular component category (Figure 8a), suggesting possible functions of OsSCYL2 in the vesicle transport pathway. Moreover, concordant with phenotypes such as ROS, antimicrobial compounds accumulation and enhanced decease resistance observed in *scyl2* (Figures 4a–f and 5a,b) or *spl28* mutants (Qiao et al., 2010), DEGs were most significantly enriched in 'secondary metabolic process' (14 genes involved) and 'oxidoreductase activity' (24 genes involved) in biological process category and molecular function category, respectively (Figure 8b,c and Tables S5, S6).

The significant enriched GO pathways were selected by using Fisher's extract test, and the threshold of significance was defined by $p \leq 0.01$.

4 | DISCUSSION

LMMs have been widely implicated in HR-mediated cell death and defence responses in plants (Bruggeman et al., 2015; Zhu et al., 2020). Although their underlying genes belong to various genetic pathways, LMMs in rice shared many common physiological and growth phenotypes, such as the spotted leaf, ROS accumulation, defects in chloroplast activity and enhanced disease resistance (Bruggeman et al., 2015; Zhu et al., 2020). So far, only a small number of LMMs have been reported to be involved in vesicle trafficking-mediated cell death and defence response in rice. These include *spl35*, *δ-cop1*, *δ-cop2*, *lrd6-6*, *sec3a*, *rls2*, *spl28* and *scyl2* (this study). Although these LMMs have defects at different stages of intercellular cargo transportation (e.g., COPI-, clathrin-coated and MVB-related vesicle trafficking), they share similar HR-like cell death and autoimmunity-related phenotypes. It is tempting to speculate that different types of vesical trafficking may crosstalk and converge to the same molecular process in the regulation of plant immunity.

SCYL2 is evolutionally conserved and was reported to play a critical role in the normal functioning of the nervous system in animals (Gingras et al., 2015; Pelletier, 2016), and mainly to regulate growth and development in *Arabidopsis* (Jung et al., 2017). Here, we show that OsSCYL2 interacts with CMVT and modulates plant immunity in rice (Figure 9). The OsSCYL2-mediated plant immunity likely requires direct binding to clathrin heavy chain OsCHC1 to facilitate interaction with OsSPL28 (clathrin AP adaptor unit). In support of this interpretation, directly blocking clathrin activities using chemical compounds (Pitstop 1 and Pitstop 2) can interfere with the pathogenic activity and protect cells against invasion (Von Kleist et al., 2011). We also find that the CHC1-centric interacting module

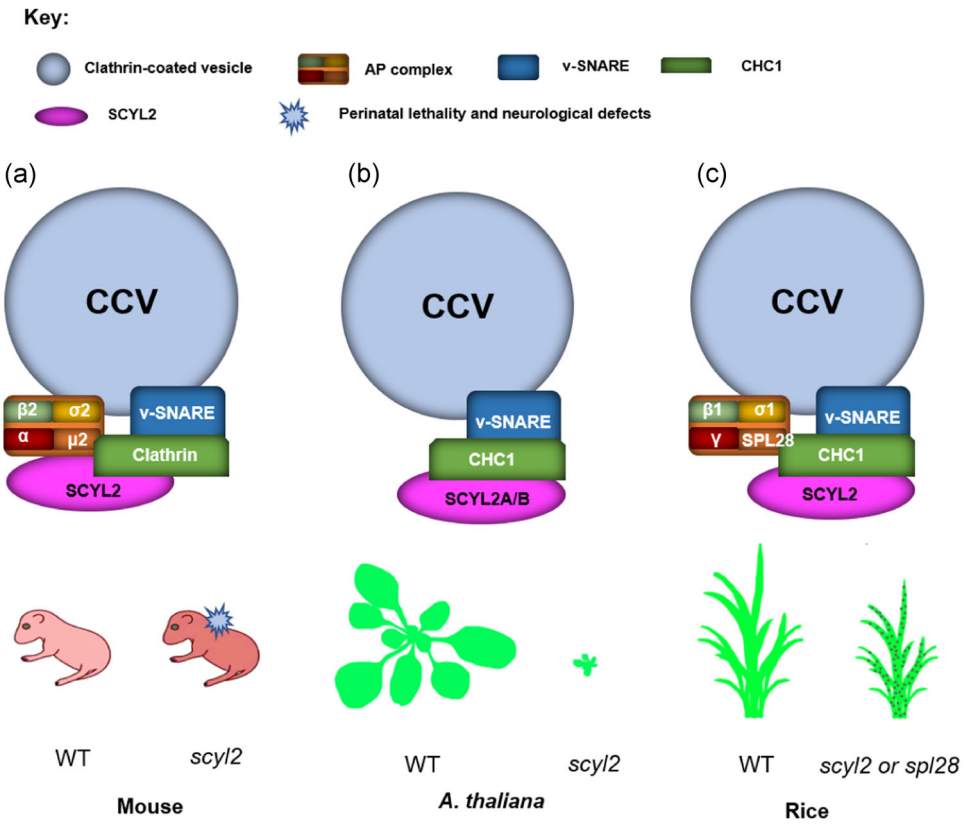

FIGURE 9 Divergent biological functions of SCYL2 in mouse, *Arabidopsis* and rice. (a) SCYL2, by directly binding to both clathrin and the clathrin-associated adaptor protein complex 2 (AP2), plays a critical role for the normal functioning of the nervous system in mouse (Conner & Schmid, 2005; Gingras et al., 2015; Pelletier, 2016). (b) SCYL2A and SCYL2B are functionally redundant and essential for plant growth and development, and directly binds to CHC1 in *Arabidopsis* (Jung et al., 2017). (c) OsSCYL2–OsSPL28 interaction is mediated by OsCHC1, and is involved in plant immunity [Color figure can be viewed at wileyonlinelibrary.com]

is likely conserved in mice, *A. thaliana* and rice, supported by in vitro or in vivo protein–protein interaction assays (Figures 7a–c and 9; Conner & Schmid, 2005, Jung et al., 2017). In rice, AP1 complex subunit OsSPL28 is the first reported CMVT-associated component in the regulation of plant cell death and immunity (Qiao et al., 2010). Isolation and characterisation of *OsSCYL2* in this study further strengthen that the CCV pathway is involved in HR-like cell death.

Based on ours results and those findings reported previously, we proposed a working model (Figure S7) for the role of OsSCYL2–OsCHC1–OsSPL28 interacting module in rice immunity. Plants have evolved an elaborate system to coordinate growth and defence response tradeoff upon biotic stress (Huot et al., 2014). In rice, the OsSCYL2–OsCHC1–OsSPL28-mediated CMVT probably function as a valve to keep the defence response at a dormant state under normal growth conditions. Mutations in *OsSCYL2* or *OsSPL28* lead to a reduction in photosynthesis activity, chloroplast damage and excessive ROS accumulation. It is reasonable that chloroplast damage occurs before ROS accumulation, since the defective phenotype of the *scyl2-1* mutant is light-dependent. The chloroplast-derived ROS probably as a key to trigger defence response (Bruggeman et al., 2015; Zurbriggen et al., 2010). However, the molecular links between the OsSCYL2–OsCHC1–OsSPL28-mediated CMVT and chloroplast integrity still need to be elucidated (Figure S7).

Balancing of yield and resistance is vital for crop cultivation and ensure food security. Mutations in LMM genes help plants to enhance resistance but at the same time adversely affect the growth and proliferation of plants. With increasing identification of LMM mutant genes over the years, coupled with the elucidation of their roles in growth and immunity, may allow manipulation of the pathways involved to achieve high yield and enhanced resistance in crops.

ACKNOWLEDGEMENTS

The authors thank Miss Longjiao Chen and Mr. Zhongyong Luo for rice plant growth and fieldwork. This study was supported by the Agriculture Research System of Shanghai (Grant No. 202103), China Postdoctoral Science Foundation (2021M692146), Shanghai Science and Technology Innovation Action Plan Project (21N11900100), Shanghai Pujiang Program (20PJ1405900) and Shanghai Technology Research Leader Program (18XD1424300).

CONFLICT OF INTERESTS

The authors declare that there are no conflict of interests.

DATA AVAILABILITY STATEMENT

The data that support the findings of this study are available from the corresponding author upon reasonable request.

ORCID

Huangwei Chu http://orcid.org/0000-0001-8846-2506

REFERENCES

Akamatsu, A., Wong, H.L., Fujiwara, M., Okuda, J., Nishide, K., Uno, K., et al. (2013) An OsCEBiP/OsCERK1-OsRacGEF1-OsRac1 module is an essential early component of chitin-induced rice immunity. *Cell Host & Microbe*, 13(4), 465–476.

Benjamini, Y. & Hochberg, Y. (1995) Controlling the false discovery rate: a practical and powerful approach to multiple testing. *Journal of the Royal Statistical Society: Series B (Methodological)*, 57(1), 289–300.

Borner, G.H., Rana, A.A., Forster, R., Harbour, M., Smith, J.C. & Robinson, M.S. (2007) CVAK104 is a novel regulator of clathrin-mediated SNARE sorting. *Traffic*, 8(7), 893–903.

Bruggeman, Q., Raynaud, C., Benhamed, M. & Delarue, M. (2015) To die or not to die? Lessons from lesion mimic mutants. *Frontiers of Plant Science*, 6, 24.

Chu, H., Liang, W., Li, J., Hong, F., Wu, Y., Wang, L., et al. (2013) A CLE-WOX signalling module regulates root meristem maintenance and vascular tissue development in rice. *Journal of Experimental Botany*, 64(17), 5359–5369.

Coll, N.S., Epple, P. & Dangl, J.L. (2011) Programmed cell death in the plant immune system. *Cell Death & Differentiation*, 18(8), 1247–1256.

Conner, S.D. & Schmid, S.L. (2005) CVAK104 is a novel poly-L-lysine-stimulated kinase that targets the beta2-subunit of AP2. *Journal of Biological Chemistry*, 280(22), 21539–21544.

Cui, Y., Peng, Y., Zhang, Q., Xia, S., Ruan, B., Xu, Q., et al. (2021) Disruption of EARLY LESION LEAF 1, encoding a cytochrome P450 monooxygenase, induces ROS accumulation and cell death in rice. *The Plant Journal*, 105(4), 942–956.

Dietrich, R.A., Delaney, T.P., Uknes, S.J., Ward, E.R., Ryals, J.A. & Dangl, J.L. (1994) *Arabidopsis* mutants simulating disease resistance response. *Cell*, 77(4), 565–577.

Draghici, S., Khatri, P., Tarca, A.L., Amin, K., Done, A., Voichita, C., et al. (2007) A systems biology approach for pathway level analysis. *Genome Research*, 17(10), 1537–1545.

Fujisaki, K., Abe, Y., Ito, A., Saitoh, H., Yoshida, K., Kanzaki, H., et al. (2015) Rice Exo70 interacts with a fungal effector, AVR-Pii, and is required for AVR-Pii-triggered immunity. *The Plant Journal*, 83(5), 875–887.

Fujiwara, T., Maisonneuve, S., Isshiki, M., Mizutani, M., Chen, L., Wong, H.L., et al. (2010) Sekiguchi lesion gene encodes a cytochrome P450 monooxygenase that catalyzes conversion of tryptamine to serotonin in rice. *Journal of Biological Chemistry*, 285(15), 11308–11313.

Gingras, S., Earls, L.R., Howell, S., Smeyne, R.J., Zakharenko, S.S. & Pelletier, S. (2015) SCYL2 protects CA3 pyramidal neurons from excitotoxicity during functional maturation of the mouse hippocampus. *Journal of Neuroscience*, 35(29), 10510–10522.

Gomez-Navarro, N. & Miller, E. (2016) Protein sorting at the ER-Golgi interface. *Journal of Cell Biology*, 215(6), 769–778.

Gong, P., Luo, Y., Huang, F., Chen, Y., Zhao, C., Wu, X., et al. (2019) Disruption of a Upf1-like helicase-encoding gene OsPLS2 triggers light-dependent premature leaf senescence in rice. *Plant Molecular Biology*, 100(1-2), 133–149.

Gu, Y., Zavaliev, R. & Dong, X. (2017) Membrane trafficking in plant immunity. *Molecular Plant*, 10(8), 1026–1034.

Hopkins, M., Taylor, C., Liu, Z., Ma, F., McNamara, L., Wang, T.W. et al. (2007) Regulation and execution of molecular disassembly and catabolism during senescence. *New Phytologist*, 175(2), 201–214.

Huot, B., Yao, J., Montgomery, B.L. & He, S.Y. (2014) Growth–defense tradeoffs in plants: a balancing act to optimize fitness. *Molecular Plant*, 7(8), 1267–1287.

Jung, J.Y., Lee, D.W., Ryu, S.B., Hwang, I. & Schachtman, D.P. (2017) SCYL2 genes are involved in clathrin-mediated vesicle trafficking and essential for plant growth. *Plant Physiology*, 175(1), 194–209.

Liu, J., Park, C.H., He, F., Nagano, M., Wang, M., Bellizzi, M., et al. (2015) The RhoGAP SPIN6 associates with SPL11 and OsRac1 and negatively regulates programmed cell death and innate immunity in rice. *PLoS Pathogens*, 11(2), e1004629.

Liu, X., Li, F., Tang, J., Wang, W., Zhang, F., Wang, G., et al. (2012) Activation of the jasmonic acid pathway by depletion of the hydroperoxide lyase OsHPL3 reveals crosstalk between the HPL and AOS branches of the oxylipin pathway in rice. *PLoS One*, 7(11), e50089.

Love, M.I., Huber, W. & Anders, S. (2014) Moderated estimation of fold change and dispersion for RNA-seq data with DESeq2. *Genome Biology*, 15(12), 550.

Ma, J., Chen, J., Wang, M., Ren, Y., Wang, S., Lei, C., et al. (2018) Disruption of OsSEC. 3A increases the content of salicylic acid and induces plant defense responses in rice. *Journal of Experimental Botany*, 69(5), 1051–1064.

Ma, J., Wang, Y., Ma, X., Meng, L., Jing, R., Wang, F., et al. (2019) Disruption of gene SPL35, encoding a novel CUE domain-containing protein, leads to cell death and enhanced disease response in rice. *Plant Biotechnology Journal*, 17(8), 1679–1693.

Martinez-Ballesta, M.C., Garcia-Ibañez, P., Yepes-Molina, L., Rios, J.J. & Carvajal, M. (2018) The expanding role of vesicles containing aquaporins. *Cells*, 7(10), 179.

McMahon, H.T. & Mills, I.G. (2004) COP and clathrin-coated vesicle budding: different pathways, common approaches. *Current Opinion in Cell Biology*, 16(4), 379–391.

Miller, G., Suzuki, N., Ciftci-Yilmaz, S. & Mittler, R. (2010) Reactive oxygen species homeostasis and signalling during drought and salinity stresses. *Plant, Cell & Environment*, 33(4), 453–467.

Paul, P., Simm, S., Mirus, O., Scharf, K.D., Fragkostefanakis, S. & Schleiff, E. (2014) The complexity of vesicle transport factors in plants examined by orthology search. *PLoS One*, 9(5), e97745.

Pelletier, S. (2016) SCYL pseudokinases in neuronal function and survival. *Neural Regeneration Research*, 11(1), 42–44.

Qiao, Y., Jiang, W., Lee, J., Park, B., Choi, M.S., Piao, R., et al. (2010) SPL28 encodes a clathrin-associated adaptor protein complex 1, medium subunit micro 1 (AP1M1) and is responsible for spotted leaf and early senescence in rice (*Oryza sativa*). *New Phytologist*, 185(1), 258–274.

Rao, Y., Jiao, R., Wu, X., Wang, S., Ye, H., Li, S., et al. (2020) SPL36 encodes a receptor-like protein kinase precursor and regulates programmed cell death and defense responses in rice. *Rice*, 14(34), 34.

Sutter, J.U., Campanoni, P., Blatt, M.R. & Paneque, M. (2006) Setting SNAREs in a different wood. *Traffic*, 7(6), 627–638.

Tian, D., Yang, F., Niu, Y., Lin, Y., Chen, Z., Li, G., et al. (2020) Loss function of SL (sekiguchi lesion) in the rice cultivar Minghui 86 leads to enhanced resistance to (hemi)biotrophic pathogens. *BMC Plant Biology*, 20(1), 507.

Tong, X., Qi, J., Zhu, X., Mao, B., Zeng, L., Wang, B., et al. (2012) The rice hydroperoxide lyase OsHPL3 functions in defense responses by modulating the oxylipin pathway. *The Plant Journal*, 71(5), 763–775.

Ueno, Y., Yoshida, R., Kishi-Kaboshi, M., Matsushita, A., Jiang, C.J., Goto, S., et al. (2015) Abiotic stresses antagonize the rice defence pathway through the tyrosine-dephosphorylation of OsMPK6. *PLoS Pathogens*, 11(10), e1005231.

Von Kleist, L., Stahlschmidt, W., Bulut, H., Gromova, K., Puchkov, D., Robertson, M.J., et al. (2011) Role of the clathrin terminal domain in regulating coated pit dynamics revealed by small molecule inhibition. *Cell*, 146(3), 471–484.

Wang, S., Lei, C., Wang, J., Ma, J., Tang, S., Wang, C., et al. (2017) SPL33, encoding an eEF1A-like protein, negatively regulates cell death and defense responses in rice. *Journal of Experimental Botany*, 68(5), 899–913.

Wang, Z., Wang, Y., Hong, X., Hu, D., Liu, C., Yang, J., et al. (2015) Functional inactivation of UDP-N-acetylglucosamine pyrophosphorylase 1 (UAP1) induces early leaf senescence and defence responses in rice. *Journal of Experimental Botany*, 66(3), 973–987.

Wellburn, A.R. (1994) The spectral determination of chlorophylls a and b, as well as total carotenoids, using various solvents with spectrophotometers of different resolution. *Journal of Plant Physiology*, 144(3), 307–313.

Yamanouchi, U., Yano, M., Lin, H., Ashikari, M. & Yamada, K. (2002) A rice spotted leaf gene, *Spl7*, encodes a heat stress transcription factor protein. *Proceedings of the National Academy of Sciences of United States of America*, 99(11), 7530–7535.

Yan, M., Zhou, S.R. & Xue, H.W. (2015) CRISPR primer designer: design primers for knockout and chromosome imaging CRISPR-Cas system. *Journal of Integrative Plant Biology*, 57(7), 613–617.

Yin, Z., Chen, J., Zeng, L., Goh, M., Leung, H., Khush, G.S. et al. (2000) Characterizing rice lesion mimic mutants and identifying a mutant with broad-spectrum resistance to rice blast and bacterial blight. *Molecular Plant-Microbe Interactions*, 13(8), 869–876.

Zeng, L.R., Qu, S., Bordeos, A., Yang, C., Baraoidan, M., Yan, H., et al. (2004) Spotted leaf11, a negative regulator of plant cell death and defense, encodes a U-box/armadillo repeat protein endowed with E3 ubiquitin ligase activity. *The Plant Cell*, 16(10), 2795–2808.

Zeng, M., Liu, S., Yang, M., Zhang, Y., Liang, J., Wan, X. et al. (2013) Characterization of a gene encoding clathrin heavy chain in maize up-regulated by salicylic acid abscisic acid and high boron supply. *International Journal of Molecular Sciences*, 14(7), 15179–15198.

Zhang, H., Zhang, J., Wei, P., Zhang, B., Gou, F., Feng, Z., et al. (2014) The CRISPR/Cas9 system produces specific and homozygous targeted gene editing in rice in one generation. *Plant Biotechnology Journal*, 12(6), 797–807.

Zhang, Y., Liu, Q., Zhang, Y., Chen, Y., Yu, N., Cao, Y., et al. (2019) LMM24 encodes receptor-like cytoplasmic kinase 109, which regulates cell death and defense responses in rice. *International Journal of Molecular Sciences*, 20(13), 3243.

Zheng, Y., Xu, J., Wang, F., Tang, Y., Wei, Z., Ji, Z., et al. (2021) Mutation types of CYP71P1 cause different phenotypes of mosaic spot lesion and premature leaf senescence in rice. *Frontiers in Plant Science*, 12488, 409.

Zhu, X., Yin, J., Liang, S., Liang, R., Zhou, X., et al. (2016) The multivesicular bodies (MVBs)-localized AAA ATPase LRD6-6 inhibits immunity and cell death likely through regulating MVBs-mediated vesicular trafficking in rice. *PLoS Genetics*, 12(9), e1006311.

Zhu, X., Ze, M., Chern, M., Chen, X. & Wang, J. (2020) Deciphering rice lesion mimic mutants to understand molecular network governing plant immunity and growth. *Rice Science*, 27(4), 278–288.

Zurbriggen, M.D., Carrillo, N. & Hajirezaei, M.R. (2010) ROS signaling in the hypersensitive response: when, where and what for? *Plant Signaling & Behavior*, 5(4), 393–396.

Zurbriggen, M.D., Carrillo, N., Tognetti, V.B., Melzer, M., Peisker, M., Hause, B. et al. (2009) Chloroplast-generated reactive oxygen species play a major role in localized cell death during the non-host interaction between tobacco and *Xanthomonas campestris* pv. *vesicatoria*. *The Plant Journal*, 60(6), 962–973.

SUPPORTING INFORMATION

Additional supporting information may be found in the online version of the article at the publisher's website.

How to cite this article: Yao, Y., Zhou, J., Cheng, C., Niu, F., Zhang, A., Sun, B. et al. (2022). A conserved clathrin-coated vesicle component, OsSCYL2, regulates plant innate immunity in rice. *Plant, Cell & Environment*, 45, 542–555. https://doi.org/10.1111/pce.14240